



Saber-Samandari, S., Gross, K. A., (2009). Nanoindentation reveals mechanical properties within thermally sprayed hydroxyapatite coatings.

Originally published in *Surface and Coatings Technology*, 203 (12), 1660-1664

Available from:

<http://dx.doi.org/10.1016/j.surfcoat.2008.12.025>

Copyright © 2008 Elsevier B.V. All rights reserved.

This is the author's version of the work. It is posted here with the permission of the publisher for your personal use. No further distribution is permitted. If your library has a subscription to this journal, you may also be able to access the published version via the library catalogue.



Nanoindentation reveals mechanical properties within thermally sprayed hydroxyapatite coatings

Saeed Saber-Samandari, Kārlis A. Gross

Abstract

Nanoindentation offers a unique capability to assess the mechanical properties of polished cross-sections of thermal spray coatings. This study set out to investigate the suitability of nanoindentation to extend the analysis of the cross-section to multiple points for a more detailed insight into variations through the thickness of the coating. Hydroxyapatite (HAp) was classified to three different particle sizes (20–40, 40–60 and 60–80 μm) and then thermally sprayed to produce a structurally homogeneous coating. Micro-Raman Spectroscopy (MRS) revealed dehydroxylation of the powder during the traverse in the thermal zone. Multiple indentations with a separation of 4 μm showed a transition within the thickness of the coating. Use of smaller particles led to higher hardness and elastic modulus compared to powder containing larger particles. The mechanical property profile provides valuable information for optimizing the processing of such coatings and feedback for the design of coating properties.

Keywords: Hydroxyapatite coatings, Micromechanical properties, Nanoindentation

1. Introduction

Nanoindentation allows numerous mechanical property assessments to be made on a single material. While the first tests were conducted on homogeneous materials [1,2], testing can also assess material assemblies from a number of materials that may be in different stress states. As a result, nanoindentation has the ability to examine materials produced from non-uniform or non-equilibrium processing conditions. This offers a unique capability to extend the understanding of engineered materials.

There is a potential to explore thermal sprayed coatings in more detail than previously reported in the literature, where larger indentations, greater than 10 μm , were made with micro-Vickers testing. The use of a sharper indenter, such as the Berkovich indenter, provides a sharper tip and allows the use of smaller indentations to produce sufficient plastic deformation and reveal mechanical properties from a smaller volume of material. Nanoindentation has the potential to be used as a probing tool to determine the change in mechanical properties through the thickness of the coating.

The recommended sample surface is a flat polished surface. Few materials will be completely flat and so a surface modification is required to establish a flat surface. This is most commonly done by grinding, followed by a series of polishing stages. This type of flat surface is routinely prepared for analysis of the coating microstructure. The only modification that may be necessary will be to avoid the use of a napped cloth that can provide relief around harder components in the coating. The cross-section

will be used to investigate the capability of nanoindentation to reveal information about the mechanical properties of the coating.

Thermal-spraying is conventionally used by the medical industry to produce bioactive coatings from HAp [3–8]. In this method, particles are melted at high temperatures and accelerated towards the substrate. When these well melted particles or 'droplets' of various sizes impact on the substrate at high velocity, they become flattened and stock together to build up a coating. However, imperfections may occur due to non-molten particles, inappropriate velocity of impact or even substrate oxidation. Further, the high temperature in this process leads to phase transformation, which can decrease the degree of crystallinity of the coating. Such a change in the microstructure may reduce the coating stability, increasing the potential for clinical failure of the implant [9]. These phenomena can cause significant variations in the overall micromechanical values throughout the coating thickness [10–13].

The coatings in this study do not contain decomposition phases or amorphous phases that can be observed on commercially used medical devices [14]. This paper will measure the micromechanical properties, both hardness and elastic modulus, of the crystalline coating. This paper will also reveal the importance of particle size in dictating the mechanical properties of the coating. To date, no research has comprehensively centered on the effect of particle size on mechanical properties of the coating.

2. Materials and methods

Polished Ti coupons were coated with hydroxyapatite using a Metco 5P flame spray torch (Sulzer Metco, Wohlen, Switzerland). The spray dried powder supplied by CAM Implants was classified by dry

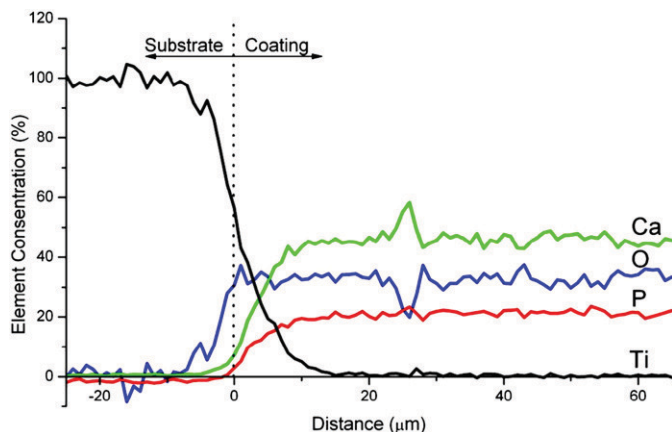


Fig. 1. Compositional profile curves of the main elements of sprayed HAp on Ti.

sieving to three different particle sizes (20–40, 40–60 and 60–80 μm). This small particle size range was chosen to provide a similar thermo kinetic history for each particle, according to previously conducted studies [15]. To ensure that droplets possessed a rounded disk shape without splashing, the Ti was preheated to 200 °C with the flame spray torch prior to spraying [16]. The spray distance was 8, 10 and 12 cm for the 20–40, 40–60 & 60–80 μm powder, respectively.

The specimens were embedded in epoxy resin, the ground and polished for indentation. Microstructures and elemental compositions of the cross-section of the samples were studied using XL30 Philips Scanning Electron Microscopy (SEM). The samples were coated with a carbon film using an Edwards S150B Sputter Coater for examination with the SEM at 20 keV. Each sample was viewed at 2000×.

Raman spectroscopy has been conducted to identify the different phases within the microstructure. The spectrum was obtained using a Raman Renishaw RM1000 micro spectrometer. Microstructural features were identified on a microscope with a 100x microscope objective. Analysis was conducted with an excitation wavelength of 514 nm at a spectral resolution of 1 cm⁻¹.

Nanoindentation was performed using a NanoTest instrument (Micro Materials Ltd. Wrexham, UK) on the cross-sectional surfaces of three samples. The indentations were conducted using the load control mode, where the load is applied and then released after the set peak load. An initial load of 0.01 mN is used for locating the surface with the Berkovich indenter, after which a loading rate of 10% of the applied load is applied. A dwell time of 5 s is used at the maximum load and a period of 60 s held at 90% of the unloaded condition for thermal drift correction. Three different loads, 50, 150 and 300 mN were applied.

Calibration of the area function was performed on the fused silica (FS) standard to confirm both the quality of the measurements and improve the measurement accuracy. FS is normally used for calibration due to its low modulus to hardness ratio. Also, mechanical properties of FS are independent of depth of indentation. Hence, series of indentation were made with loads ranging from 50 to 300 mN. The hardness and elastic modulus of FS, assuming a Poisson's ratio of 0.165, were measured to be 8.86±0.07 and 72.12±0.25 GPa, respectively.

The slope of the unloading curve can be used as a measure of the elastic properties of the sample [17]

$$E_r = \frac{\sqrt{\pi}S}{2\sqrt{A}}$$

where S is the slope of the initial portion of the unloading curve, A is the projected area and E_r is the reduced modulus defined by:

$$\frac{1}{E_r} = \frac{1-\nu_s^2}{E_s} + \frac{1-\nu_i^2}{E_i}$$

Where E_s and ν_s are elastic modulus and Poisson's ratio for the sample, and E_i and ν_i are the same parameters for the indenter. It is noted that the Poisson's ratio and elastic modulus of the diamond indenter are 0.07 and 1141 GPa, respectively [18]. In this study, the upper 60% of the unloading curve was chosen to determine the elastic modulus.

3. Results and discussion

3.1. Elemental analysis

The qualitative SEM-line analysis shows that the oxygen content is uniform in the through-thickness direction from the coating surface to the Ti-HAp interface, Fig. 1. This oxygen concentration is in accordance to that required for HAp. A closer examination reveals that both the calcium and phosphorus concentration begins to decrease at 10 μm from the interface. This suggests that the oxygen present would be present for the HAp, but also the Ti that appears to have diffused into the coating. This diffusion is a consequence of preheating the Ti with the flame before application of the coating. The ease of accommodating foreign ions by the HAp structure will modify the properties of the coating adjacent to the Ti substrate, and this will have a direct effect on the mechanical properties within the 10 μm layer from the interface. Thermal energy of the ceramic particle upon impact can also produce compositional and structural changes in the metal surfaces that can alter the mechanical properties of the substrate [19].

Modification of crystal structure of HAp within the rest of the coating from thermal spraying has not been addressed, but it is expected that the mechanical properties will change in response to an alteration of the chemistry in the apatite. Dehydroxylation of HAp will probably not have an easily quantifiable effect due to random positioning of vacancy defects, O²⁻ and OH⁻ within the crystal structure.

3.2. Calcium phosphate characterization

The coating is free of decomposition phases, and has a preferred orientation with the c -axis perpendicular to the surface of the coating (as determined by X-ray diffraction, not shown here). The selection of flame spraying was intentional to lower the possibility of phase decomposition. Micro-Raman spectra were recorded within the range of 800 and 1200 cm⁻¹ where the most intense peaks for the amorphous/crystalline phases appear [20]. Fig. 2 shows a double peak in the Raman spectra of three samples in the region of 700 to 1200 cm⁻¹. A peak at this position has traditionally been assigned to an amorphous phase [21], but closer inspection reveals that the reported peak is narrower. The narrower band located at 949 cm⁻¹ is most probably due to oxyapatite or an oxyhydroxyapatite.

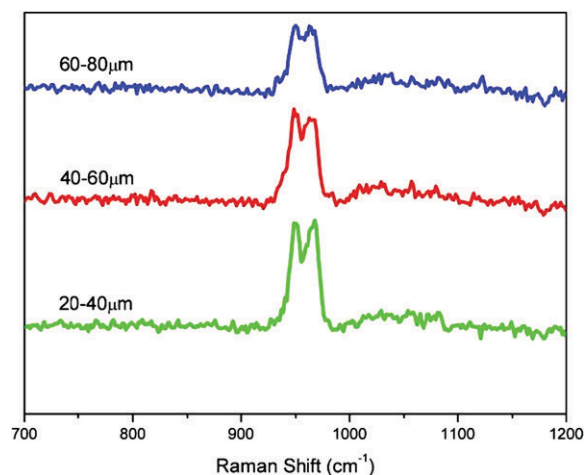


Fig. 2. Micro-Raman spectra of coatings produced from different particle size feedstock.

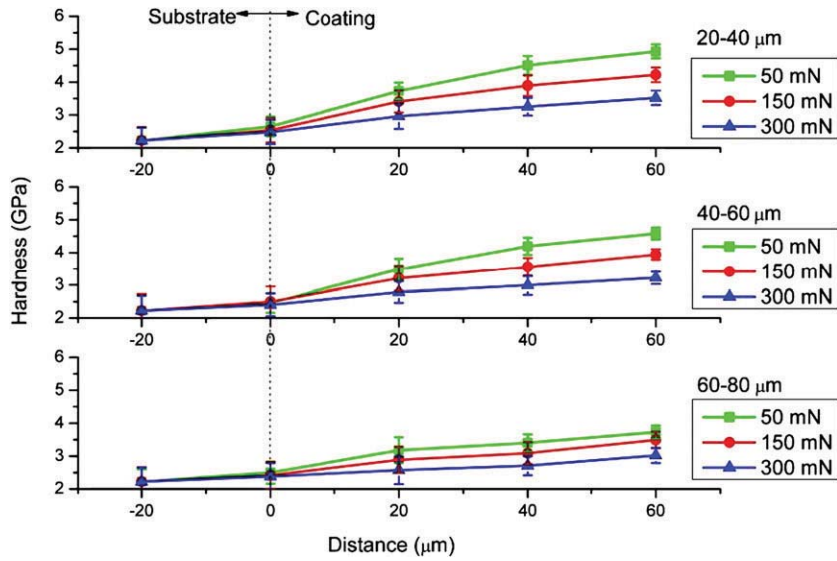


Fig. 3. Hardness of coating cross-sections from different sized feedstock. A load of 50 mN produced $\sim 6.5 \mu\text{m}$ sized indentations in HAp.

A second peak is located at about 960 cm^{-1} , a band that has been known to occur in HAp [20,21]. It is slightly displaced to higher wave numbers. The coating made from the smallest particles has a narrow peak at 968 cm^{-1} , but coatings made from medium and large particles have a peak at 963 cm^{-1} , Fig. 2.

This change in peak position could arise from a stress on the coating. Studies by Xu et al. [22] have reported an increased wave number from 960 to 970 cm^{-1} when fluorapatite is placed into compression. HAp has a slightly lower elastic modulus than fluorapatite and thus a larger peak shift will occur under the same applied stress. The peak shift from the micro-Raman spectra in Fig. 2 suggests the presence of a compression stress within the coating.

3.3. Micromechanical properties

3.3.1. Hardness

The hardness was determined at five points on each coating's cross-section from the Ti substrate to the HA coating with a $20 \mu\text{m}$ spacing, Fig. 3. Within the titanium substrate, the hardness remains constant at about 2.2 GPa regardless of the testing conditions. Within

the HAp coating, the hardness increases at a constant rate towards the surface of the coating. There is a further change caused by the indenter load, showing an additional increase in hardness with a smaller load [23]. For example, the hardness at the surface on the coating made from 20–40 μm sized powder is 4.9, 4.2 or 3.5 GPa with an indenter load of 50, 150 or 300 mN, respectively. This variation is less pronounced with coatings produced from a larger particle size feedstock. The coating made from 60–80 μm powder has a hardness of 3.7, 3.5 and 3.0 when tested with an indenter load 50, 150 and 300 mN, respectively. Values increase gradually with distance from the substrate with a steeper gradient in the coating made from smaller particles. This hardness behaviour is comparable to recent studies on plasma sprayed coatings [10,24]. The value of approximately 5 GPa agrees with indentation number 45, on the center of the splat, taken from the surface of the coating [25]. Cheng et al. used laser melting of hydroxyapatite to form a coating and also found that the hardness increased from 2.5 GPa at the substrate to 7 GPa at the coating surface [10]. This increase in hardness is common to both laser melted and thermally sprayed hydroxyapatite.

An array of indentations made in the mounting epoxy, coating and metallic substrate produced similar-sized indentations in the Ti and HAp, and larger indentations in the epoxy. An environmental scanning electron microscope (ESEM) was used to observe residual indentations at 1750 \times , Fig. 4. A picture of the indentation location and indent

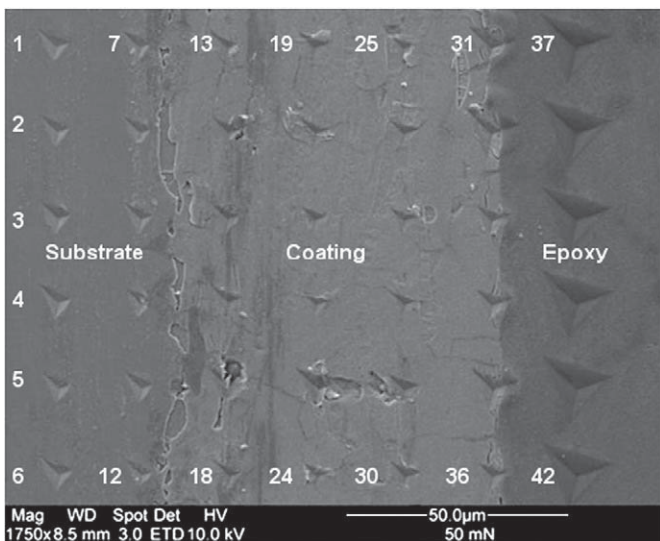


Fig. 4. Scanning electron micrograph of a grid of nanoindentations made with a Berkovich indenter in a cross-section of HAp coating on Ti. (Coatings were made from 40–60 μm powder).

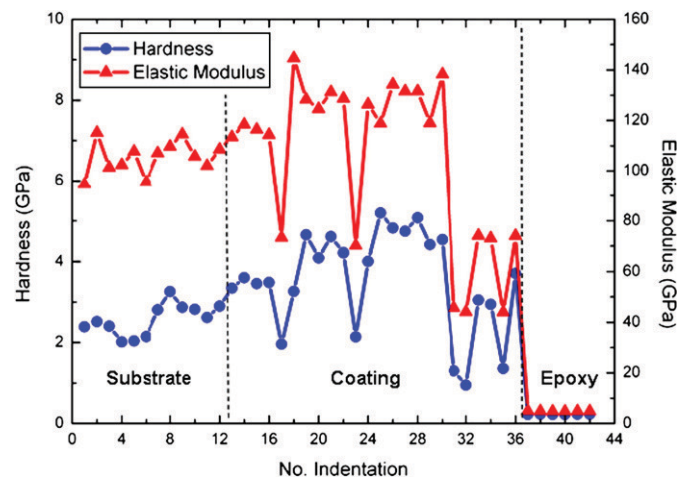


Fig. 5. Hardness and elastic modulus of indentations as shown in Fig. 5.

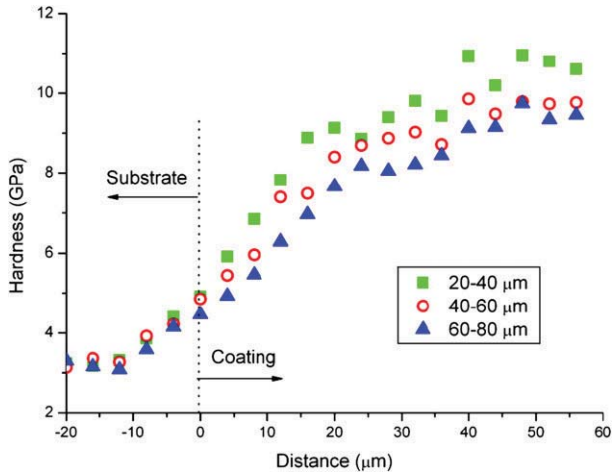


Fig. 6. Hardness vs. distance for HAp by applying a low load of 10 mN.

shape allow a direct correlation to the mechanical property value. A closer comparison of the individual values with the indent shape reveals that the low elastic modulus and hardness values reported for indents 17 and 23 can be related to porosity and cracking, respectively. Indentation 23 has supposedly been produced on a crack network that has caused dislodgement of material under the indenter. Results from indentations 17 and 23 can be omitted from the material analysis.

The elastic modulus of the titanium substrate is constant, with a natural scatter of results, but the hardness shows a slow increase within the titanium substrate, and also within the coating. Hardness reported from indentations at the coating-epoxy interface appears to be lower than the core of the coating. Correlation of the individual indentations with the numerical hardness values suggests that the epoxy has provided less rigid support compared to the hydroxyapatite. Data from indentations 1–30 are only useful for analysis and provides information from 2 depths in the titanium and 3 depths in the coating.

More indentations with a very small spacing are needed to examine the trend in more detail. Twenty indentations were performed on each sample by applying a 10 mN load which allowed indentations to be placed closer to one another, Fig. 6. This lower load is less than the critical load and so larger hardness values will result, but the additional information from smaller indentations will be useful for interpolation to understand the trend within the coating. The results

display a constant hardness in the substrate, from -20 to -10 μm , followed by a steady increase up to the interface, from -10 to 0 μm . This more detailed information confirms the increase in hardness in the substrate, but shows how the increase starts only at 10 μm from the interface and rises more steeply, than that shown in Figs. 3 and 5. The increase in hardness may be attributed to the presence of oxygen in the substrate, Fig. 1, which has also resulted in off-centre triangular indentations as observed at the interface in Fig. 4 (indentations 7–12).

3.3.2. Residual stress

Hardness has been used as an indicator of the stress state within a material [26]. It has been noted that the hardness decreases with tensile stress and increases with compressive stress, with the effect being more pronounced in tension. Therefore, overestimated values in Ti and underestimated values in HAp regions close to the HAp/Ti interface are not surprising.

The hardness increases abruptly, at 0 to 20 μm , followed by a slow increase within the 20 to 40 μm region and a plateau at 40 to 60 μm . As can be inferred from Fig. 6, one would expect that 40 μm is the critical thickness, where there is a balance of tensile and compressive residual stresses. Compressive residual stresses overestimate the hardness on the top surface, while tensile residual stresses underestimate the hardness of the coating adjacent to the substrate.

This residual stresses is expected to arise from the different coefficient of thermal expansion (CTE) of the HAp and Ti. The CTE of HAp ($15.6\text{--}16.0 \times 10^{-6} \text{ K}^{-1}$) [27,28] is higher than Ti ($8.6 \times 10^{-6} \text{ K}^{-1}$) [29], and thus, upon cooling, the HAp coatings will be subjected to a residual tensile stress. Other factors such as a change in apatite composition due to dehydroxylation and a temperature gradient within the apatite coating will modify the resulting stress condition. A different experiment needs to be conducted to completely understand the formation of the residual stress and so the generation mechanism of residual stress will not be discussed here.

3.3.3. Elastic modulus

Results show a gradual increase as the interface is approached from the substrate, Fig. 7. This could reflect the increase in the oxygen content in the substrate, as revealed in Fig. 1. A further increase occurs within the coating towards the surface of the coating. Factors that may contribute to a deviation in elastic modulus include a change in composition, from dehydroxylation, and porosity. Gross and Rodriguez-Lorenzo have reported that elastic modulus increases with increasing fluoride contents [30]. No study has been conducted on the elastic modulus of oxyapatite–hydroxyapatite solid solutions, but it is

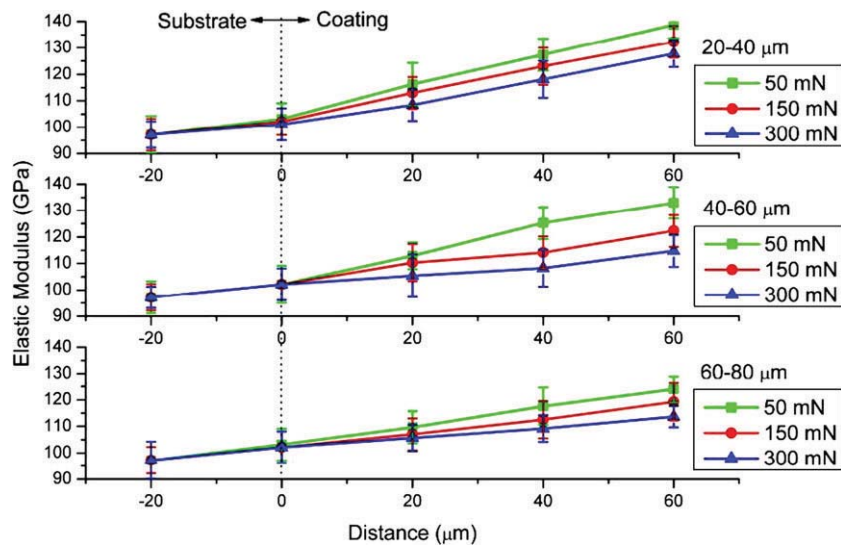


Fig. 7. Elastic modulus of HAp coatings on Ti as a function of distance from the Ti substrate to HAp top surface.

expected that the dehydroxylation will not have such a big effect as the strong electronegative fluoride. Changes in elastic modulus are not clearly understood and represent an area that requires more work, despite other reports that have disclosed the same trend [31,32].

The smaller particle size leads to a higher elastic modulus in the coating surface, regardless of the indentation load. A Poisson's ratio of 0.28 for the HAp [33] was used to calculate the elastic modulus, and this led to ~120, ~111 and ~108 GPa for the coatings made from small, medium and large particles, respectively. Obtained results are in good agreement with reported values [34–36]. These values are lower than sintered hydroxyapatite, due to the crack network in the coatings. A higher crack density or wider cracks are expected to be found in the coating made from the largest particles.

A higher hardness at the coating surface may be attributed rehydroxylation of the coating surface [37] and a smaller grain size on the surface. As a result, the use of hardness to ascertain the residual stress needs an assessment of the hydroxyl state and the grain size within the microstructure. Such an approach is tedious and requires specialized microchemical analysis tools. An alternative strategy is required. This may involve the investigation of cracking within the ceramic coating or the change in the fracture toughness resulting from the pre-stressed material. Further work will investigate other nanoindentation strategies for calculating the residual stress.

4. Conclusions

Nanoindentation testing revealed a non-uniform stress state throughout the HAp coating. The flame spray process produced a residual stresses, as revealed by an increase in hardness from the interface towards the coating surface. The use of lower loads, possible with nanoindentation, revealed this more clearly compared to higher loads that would be used with micro-hardness testing. The surface exhibited a higher hardness suggesting a compressive stress in the surface, but a tensile stress at the Ti-HAp interface.

The particle size used in the thermal spray procedure will influence the residual stress that is formed within the coating. The magnitude of the hardness for small particles (20–40 μm) was found to be 4.5 GPa, but lower at 3.9 and 3.5 GPa for medium (40–60 μm) and large sized

particles (60–80 μm), respectively. A similar trend was observed for the elastic modulus in the three coatings.

References

- [1] M.F. Doerner, W.D. Nix, *J. Mater. Res.* 1 (1986) 601.
- [2] W.C. Oliver, G.M. Pharr, *J. Mater. Res.* 7 (1992) 1564.
- [3] G.L. De Lange, K. Donath, *Biomaterials* 10 (1989) 121.
- [4] K. De Groot, R. Geesink, C.P. Klein, P. Serekian, *J. Biomed. Mater. Res.* 21 (1987) 1375.
- [5] R.J. Furlong, J.F. Osborn, *J. Bone Jt. Surg.* 73B (1991) 741.
- [6] L. Sun, C.C. Berndt, K.A. Gross, A. Kucuk, *J. Biomed. Mater. Res.* 58 (2001) 570.
- [7] B.Y. Chou, E. Chang, *Scr. Mater.* 45 (2001) 487.
- [8] C.C. Berndt, G.N. Haddad, A.J.D. Farmer, K.A. Gross, *Mater. Forum* 14 (1990) 161.
- [9] B. Koch, J. Wolke, K.D. Groot, *J. Biomed. Mater. Res.* 24 (1990) 655.
- [10] G.J. Cheng, D. Pirzada, M. Cai, P. Mohanty, A. Bandyopadhyay, *Mater. Sci. Eng., C* 25 (2005) 541.
- [11] P. Araujo, D. Chicot, M. Staia, J. Lesage, *Surf. Eng.* 21 (2005) 35.
- [12] P. Fogarassy, B. Cofino, P. Millet, A. Lodini, *IEEE Trans. Biomed. Eng.* 52 (2005) 1161.
- [13] Y.C. Tsui, C. Doyle, T.W. Clyne, *Biomaterials*, 19 (1998) 2015.
- [14] K.A. Gross, V. Gross, C.C. Berndt, *J. Am. Ceram. Soc.* 81 (1998) 106.
- [15] K.A. Gross, *Materials Engineering* (thesis), Monash University, Melbourne, Australia, 1990.
- [16] D. Muller, *Materials Engineering* (thesis), Technical University of Munich, Germany, 2004.
- [17] I.N. Sneddon, *Int. J. Eng. Sci.* 3 (1965) 47.
- [18] G. Simmons, H. Wang, *Single crystal elastic constants and calculated aggregate properties: A handbook*, MIT Press, Cambridge, MA, 1971.
- [19] P. Ducheyne, K.E. Healy, *J. Biomed. Mater. Res.* 22 (1988) 1137.
- [20] K.A. Gross, M.R. Phillips, *J. Mater. Sci., Mater. Med.* 9 (1998) 797.
- [21] K.C. Blakeslee, R.A. Condrate, *J. Am. Ceram. Soc.* 54 (1971) 559.
- [22] J. Xu, D.F.R. Gilson, I.S. Butler, I. Stangel, *J. Biomed. Mater. Res.* 30 (1996) 23.
- [23] I. Manika, J. Maniks, *Acta Mater.* 54 (2006) 2049.
- [24] P.S. Uskokovic, C.Y. Tang, C.P. Tsui, N. Ignjatovic, D.P. Uskokovic, *J. Am. Ceram. Soc.* 27 (2007) 1559.
- [25] K.A. Gross, S. Saber-Samandari, *J. Aust. Ceram. Soc.* 43 (2007) 98.
- [26] T.Y. Tsui, W.C. Oliver, G.M. Pharr, *J. Mater. Res.* 11 (1996) 752.
- [27] C.-W. Yang, T.-M. Lee, T.-S. Lui, E. Chang, *Mater. Sci. Eng., C* 26 (2006) 1395.
- [28] G.R. Fischer, P. Bardhan, G.E. Geiger, *J. Mater. Sci. Lett.* 2 (1983) 577.
- [29] S. Zinelis, A. Tsetsekou, T. Papadopoulos, *J. Prosthet. Dentistry.* 90 (2003) 332.
- [30] K.A. Gross, L.M. Rodriguez-Lorenzo, *Biomaterials.* 25 (2004) 1385.
- [31] K.A. Khor, Y.W. Gu, C.H. Quek, P. Cheang, *Surf. Coat. Technol.* 168 (2003) 195.
- [32] C.Y. Ning, Y.J. Wang, X.F. Chen, N.R. Zhao, J.D. Ye, G. Wu, *Surf. Coat. Technol.* 200 (2005) 2403.
- [33] G. DeWith, H.J.A. VanDijk, N. Hattu, K. Prijs, *J. Mater. Sci.* 16 (1981) 1592.
- [34] R.B. King, *Int. J. Solids Struct.* 23 (1987) 1657.
- [35] S. Johnson, M. Haluska, R.J. Narayan, R.L. Snyder, *Mater. Sci. Eng., C* 26 (2006) 1312.
- [36] C. Zhang, Y. Leng, J. Chen, *Biomaterials.* 22 (2001) 1357.
- [37] K.A. Gross, C.C. Berndt, P. Stephens, B. Dinnebie, *J. Mater. Sci.* 33 (1998) 3985.